DOI: 10.21062/mft.2026.025 © 2026 Manufacturing Technology. All rights reserved. http://www.journalmt.com

Study on Removal Mechanism and Surface Topography in Ultrasonic-Assisted Grinding of High Volume Fraction SiCp/Al Composite

Weicheng Guo (0000-0001-5056-4451), Hailong Zhang (0009-0007-6856-483X), Miaoxian Guo (0000-0001-7838-9704)*
School of Mechanical Engineering, University of Shanghai for Science and Technology, Shanghai, 200093, China. *Email:guomx@usst.edu.cn

High volume fraction SiCp/Al composites are highly valued in aerospace, automotive, and electronic packaging for their exceptional mechanical and thermal properties. To enhance the machinability of these difficult-to-cut materials, this study systematically evaluates ultrasonic vibration-assisted grinding (UAG) against conventional grinding (CG). Experimental comparisons reveal that UAG lowers grinding forces by up to 26%, a benefit primarily driven by the reduction in undeformed chip thickness (UCT). This kinematic modification optimizes the particle removal mode, thereby mitigating severe particle fracture and interfacial debonding. Crucially, the superior surface integrity observed with UAG results from extending the critical threshold for particle fracture, suppressing roughness accumulation at higher feed rates, and amplifying the load-relief effect of increased spindle speeds. These findings provide both theoretical insights and experimental validation for the high-efficiency machining of SiCp/Al composites.

Keywords: High volume fraction SiCp/Al, Ultrasonic vibration-assisted grinding, Grinding force, Surface topography

1 Introduction

SiCp/Al composites have attracted considerable attention owing to their high stiffness, low coefficient of thermal expansion, excellent thermal conductivity, and superior thermal stability [1], which make them promising candidates for applications in aerospace, electronic packaging, and automotive industries [2-6]. However, the pronounced mismatch in mechanical properties between the hard and brittle SiC particles and the ductile aluminum matrix poses significant challenges during machining. In particular, the high hardness, strong brittleness, and non-uniform spatial distribution of SiC particles often result in severe tool wear, elevated grinding forces, and deteriorated surface integrity. Typical surface defects, including pits, microcracks, and matrix tearing, are frequently observed after machining, which severely restricts the broader industrial application of SiCp/Al composites.

To overcome these machining difficulties, extensive efforts have been devoted to the development of advanced assisted machining techniques. Among them, ultrasonic vibration-assisted grinding (UAG) has been demonstrated to be an effective approach for mitigating particle damage, reducing grinding forces, and improving surface quality while enhancing machining efficiency. Compared with conventional grinding (CG), UAG modifies the abrasive–workpiece interaction by altering the material removal trajectory, shortening the effective contact time, and introducing periodic impact effects, thereby significantly lowering grinding forces, prolonging tool life, and improving surface finish. Yao et al. [7] reported that the introduction of axial ultrasonic vibration reduced the surface roughness Sa by 22.9% at a grinding depth of 20 μm., accompanied by a remarkable suppression of pits, voids, and crack defects. Similarly, Chen et al. [8] observed that, under an ultrasonic amplitude of 4 μm., pit-related defects were substantially alleviated, confirming the pronounced effectiveness of UAG in reducing cutting forces and surface roughness. Orthogonal experiments conducted by Gu et al. [9] further indicated that axial ultrasonic vibration plays a positive role in enhancing the surface quality of SiCp/Al composites. Jin et al. [10] investigated the influence of ultrasonic amplitude on surface roughness and revealed that, within an appropriate range, ultrasonic vibration promotes controlled fracture of SiC particles, thereby reducing pits and scratches, whereas excessive amplitude may adversely affect surface quality. In addition, Yuan et al. [11] found that UAG enables the generation of more uniform and consistent machined surfaces.

The undeformed chip thickness (UCT), which represents the ideal instantaneous cutting thickness, is widely recognized as a critical factor governing grinding force and particle removal mode. Compared with CG, UAG effectively reduces the UCT under identical machining parameters, leading to lower

grinding forces and improved surface integrity. In this context, Zhou et al. [12] investigated the relationship between critical cutting depth and UCT and elucidated its influence on particle removal mechanisms in ceramic matrix composites, experimentally confirming a significant reduction in grinding force under UAG conditions. Zhang et al. [13] developed a grinding force model for UAG by incorporating ultrasonic kinematics, chip formation mechanisms, and frictional behavior. Gao et al. [14] systematically studied the effect of UCT on material removal modes in hard and brittle materials, demonstrating that when the UCT falls below the ductile–brittle transition threshold, material removal tends to occur via plastic deformation, thereby suppressing crack initiation, a process that is further facilitated by ultrasonic assistance. To more accurately characterize UCT under ultrasonic conditions, several theoretical models have been proposed. Cheng et al. [15] established a three-dimensional UCT model for compound ultrasonic-assisted surface grinding, while Li et al. [16] incorporated the influence of grinding wheel topography by numerically simulating the dressed wheel surface to improve UCT prediction accuracy.

Following the confirmation of the performance advantages of UAG, increasing attention has been directed toward clarifying the specific differences in particle damage behavior and surface integrity between CG and UAG. Jie et al. [17] compared the damage characteristics of SiC particles under both machining methods and found that ultrasonic vibration induces microcracking within particles, facilitating shear-dominated removal and effectively reducing pit formation caused by particle pull-out. Zhou et al. [18] further demonstrated that ultrasonic vibration suppresses excessive particle fragmentation and interfacial debonding, enhances plastic material removal, and consequently reduces surface roughness. Yao et al. [19] revealed that, under periodic impact associated with elliptical ultrasonic vibration, SiC particles tend to undergo controlled micro-brittle fracture along grain boundaries or pre-existing defects at relatively lower forces. Gu et al. [9] additionally reported that improved separation between abrasive grains and the workpiece under elliptical ultrasonic motion significantly reduces subsurface damage depth in the aluminum matrix and further improves surface finish. The prediction of surface roughness was successfully implemented by Maya et al. [20] through the integration of key grinding parameters and diverse machine learning algorithms.

It should be noted that the volume fraction of SiC particles plays a decisive role in determining the mechanical properties and machinability of SiCp/Al composites. In practical applications, composites with different particle volume fractions exhibit markedly distinct machining behaviors. Nevertheless, most existing studies have primarily focused on the influence of UAG on grinding performance and surface quality using relatively low particle volume fractions, while investigations in the high volume fraction regime remain limited. To facilitate the wider engineering application of SiCp/Al composites, the present study aims to systematically investigate and compare the machining performance, grinding force characteristics, and surface integrity of high volume fraction SiCp/Al composites under conventional grinding and ultrasonic vibration-assisted grinding conditions.

2 Experimental Materials, Equipment, and Methods

2.1 Materials and Grinding Wheel

The high volume fraction SiCp/Al composites employed in this study were fabricated by powder metallurgy, consisting of an aluminum matrix reinforced with SiC particles at a volume fraction of 60%. The microstructural morphology of the composite is presented in Fig. 1(a), in which the SiC reinforcing particles exhibit an average diameter of approximately 45 μm. The detailed physical properties of the material are summarized in Table 1.Considering the sensitivity of the ultrasonic vibration platform to the mass of the workpiece during operation, the bulk composite material was sectioned into specimens with dimensions of 20 mm × 20 mm × 10 mm prior to the grinding experiments using wire electrical discharge machining, as illustrated in Fig. 4(a). To ensure consistent initial surface conditions, the specimen surfaces were pre-machined by milling and subsequently subjected to ultrasonic cleaning to obtain a flat and contamination-free surface before the formal grinding tests.

***Tab. 1** Mechanical properties of Al matrix and SiC particles*

Material	Density ρ ($kg \cdot m^{-3}$)	Elastic Modulus E (GPa)	Bending strength (MPa)	Specific Heat ($J \cdot g^{-1} \cdot K^{-1}$)	Thermal Conductivity ($W \cdot m^{-1} \cdot K^{-1}$)	Poisson rate μ
Al	2.7×10^3	71.9	325	880	193	0.34
SiC	3.2×10^3	420	1500	427	81	0.17

Considering the high hardness of SiC particles, a bronze-bonded diamond grinding wheel was selected for the experiments, as shown in Fig. 4(a). The grinding wheel has a diameter of 100 mm and a thickness of 6 mm, with a grit size of 120 mesh. The average diamond grain size is approximately 125 μm. The morphology of the abrasive grains observed under a scanning electron microscope is presented in Fig. 1(b).Prior to the formal experiments, the grinding wheel was sharpened using an 80-mesh SiC oilstone to ensure sufficient protrusion and cutting ability of the abrasive grains. During the sharpening process, the oilstone was fixed in position, while the grinding wheel rotated at a relatively low spindle speed and traversed at a higher feed rate under adequate cooling conditions. The sharpening operation was repeated multiple times until a smooth wheel surface was obtained, accompanied by a stable grinding sound without abnormal noise, indicating a well-conditioned grinding wheel.

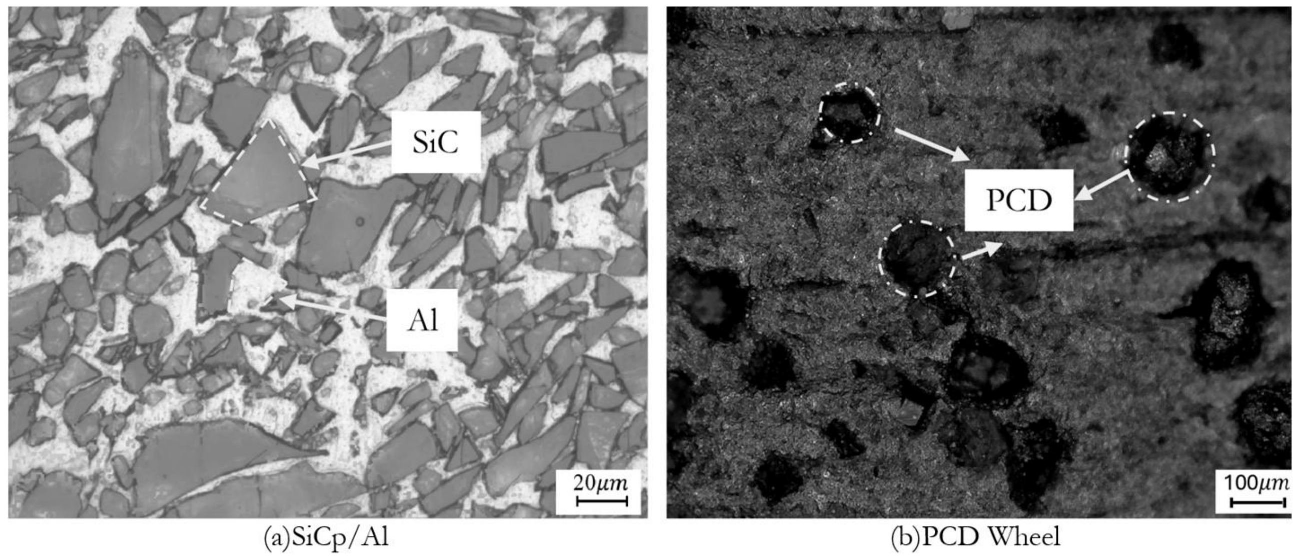

Fig. 1 *Morphology of particles and abrasive particles*

2.2 Kinematics of the Ultrasonic-Assisted Motion

A two-dimensional ultrasonic vibration mode parallel to the end face of the grinding wheel was employed in the experiments. Within a three-dimensional Cartesian coordinate system, the workpiece was subjected to ultrasonic vibrations along both the X- and Y-directions, while the relative motion of the grinding wheel axis with respect to the workpiece occurred along the X-direction. Figures 2(a) and 2(b) illustrate the front view and top view of the ultrasonic vibration-assisted grinding configuration, respectively. The grinding operation was conducted in a side-grinding mode, where v_w and v_s denote the feed speed and the linear speed of the grinding wheel, respectively.

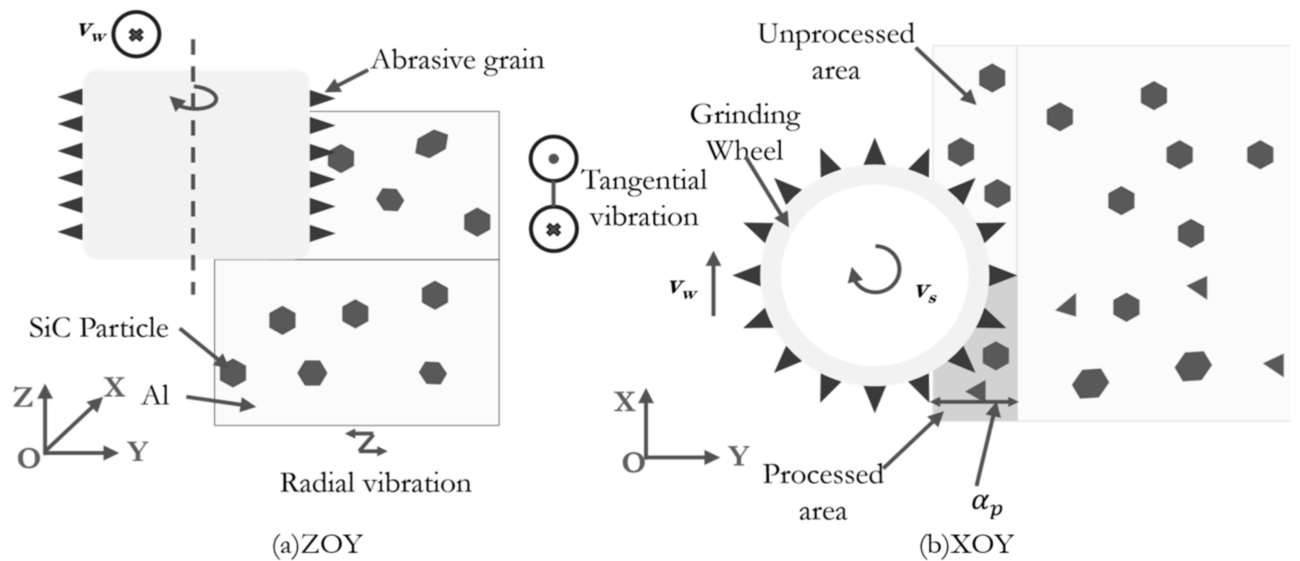

Fig. 2 *Schematic diagram of ultrasonic vibration grinding process photograph*

Under relative motion conditions, the workpiece is assumed to be stationary, and the relative motion of an individual abrasive grain is therefore attributed solely to ultrasonic vibration. Accordingly, all subsequent analyses in this study are conducted based on the assumption that the workpiece remains non-vibrating, while the abrasive grain undergoes ultrasonic motion. Figures 3(a) and 3(b) present the kinematic characteristics of a single abrasive grain without and with ultrasonic assistance, respectively. In Fig. 3, the red and orange trajectories correspond to the chip formation processes under conventional grinding (CG) and ultrasonic vibration-assisted grinding (UAG).

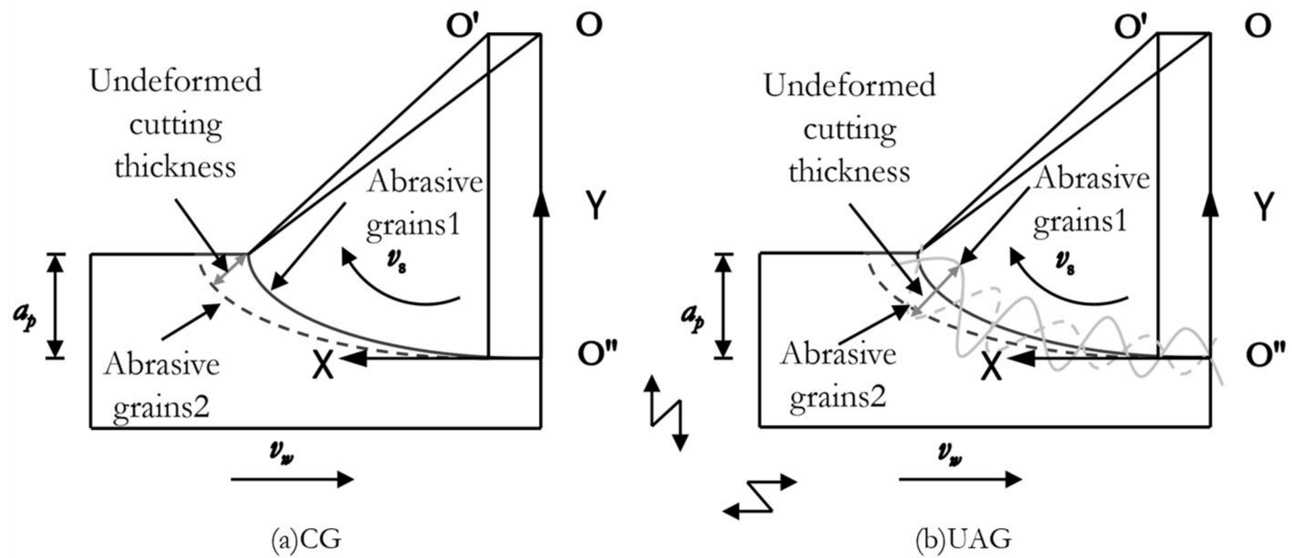

Fig. 3 *Chip formation process in the grinding arc zone*

During a single abrasive grinding process, in the XYO"coordinate system, the abrasive trajectory in UAG exhibits a regular cycloidal shape. The motion trajectory equation of a single abrasive particle is given by Equation (2-1).

$$\begin{cases} x(t) = -v_w t + R\cos(\omega t) + A_x \sin(2\pi f t) \\ y(t) = R\sin(\omega t) + A_y \cos(2\pi f t) \\ z(t) = 0 \end{cases} \tag{1}$$

The maximum undeformed chip thickness(UCT) h_{max}[21] under ultrasonic vibration is given by Equation (2-2).

$$h_{max} = \left[\frac{6}{C \cdot N_d} \cdot \frac{v_w}{v_s + v_{vib}} \cdot \sqrt{\frac{a_p}{R}}\right]^{1/2} \tag{2}$$

Where
R…Grinding wheel radius [mm],
w…Angular velocity of abrasive grain [rad·s^{-1}],
Ax…Tangential ultrasonic amplitude [μm],
Ay…Radial ultrasonic amplitude,[μm],
f…Ultrasonic frequency [kHz],
v_w…Workpiece feed speed [mm·s^{-1}],
v_s…Wheel speed [m·s^{-1}],
a_p…Grinding depth [μm],
h_{max}…Maximum undeformed chip thickness [mm],
C…Grain Shape Factor, C=0.5,
N_d…Dynamic Cutting Edge Density per Unit Area, N_d=45, [mm^{-2}],
$v_{vib:}$…Additional equivalent speed introduced by ultrasonic vibration, in elliptical ultrasonic vibration, the maximum instantaneous speed of the abrasive grain along the cutting direction increases. Typically $v_{vib} = 2\pi f A_x$.

2.3 Experimental Procedures and Parameters

The UAG experimental platform employed in this study is based on a Beijing Jingdiao Carver S600A machining center. The complete experimental system consists of the machining center, grinding tool, workpiece, ultrasonic vibration generation system, signal acquisition system, and fixture assembly, as illustrated in the machining setup shown in Fig. 4(b). The selected ultrasonic working mode is the workpiece vibration method, in which the specimen is mounted on a bidirectional ultrasonic vibration platform. The ultrasonic platform is connected to

a dynamometer (9139A, Kistler) and horizontally fixed on a magnetic fixture. Prior to the single-factor and orthogonal experiments, a laser Doppler vibrometer was used to calibrate the vibration amplitude and frequency of the ultrasonic platform. After multiple measurements and validation, the effective operating amplitudes were determined to be 5 μm. in the tangential direction and 3 μm. in the radial direction, with a vibration frequency of 20.4 kHz.During the grinding experiments, the three orthogonal components of the grinding force were acquired in real time using the dynamometer and recorded, analyzed, and visualized through Dynoware software. After the experiments, the ground surface morphology and surface roughness were characterized using a scanning electron microscope (SEM, ZEISS Gemini 300) and a white-light interferometer (Nano Surface white light interferometer, NPFLEX), respectively. The corresponding characterization instruments are shown in Fig. 4(c).

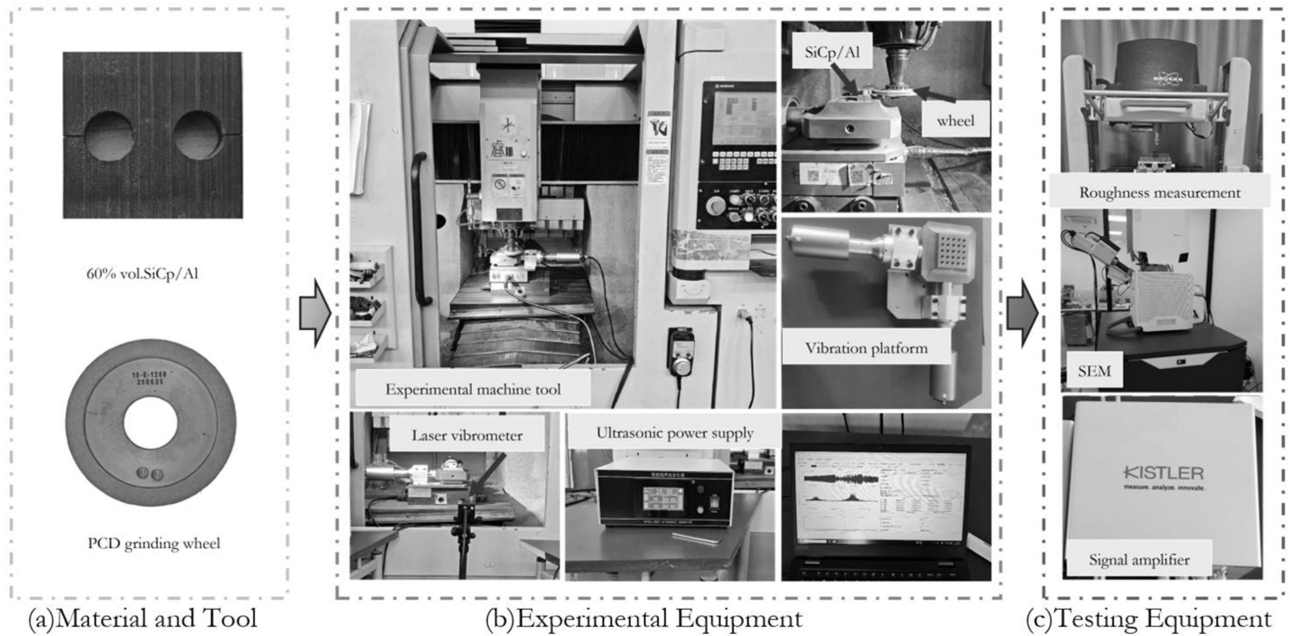

Fig. 4 *On-site Machining photograph*

The experimental study involved single-factor tests conducted separately for the CG and UAG control groups. Independent variables comprised the grinding wheel feed speed (v_w), spindle speed (v_s), grinding depth (a_p), and UCT (h_{max}). These parameters were determined by synthesizing prior literature with actual processing conditions, and their specific values are listed in Table 2.

Tab. 2 *Grinding Experimental Parameters*

$v_s(\mathrm{m \cdot s^{-1}})$	$v_w(\mathrm{mm \cdot min^{-1}})$	a_p(μm)	h_{max}(μm)
13.09, 18.33, 23.56, 28.80	50, 100, 150, 200	5, 10, 15, 20	0.33, 0.65, 0.96, 1.26

3 Test results and Analysis

3.1 Grinding Force

Grinding force acts as a core metric for evaluating the machining process, directly linking parameter settings to material removal, wheel sharpness, and ultrasonic efficacy. Consequently, investigating how grinding depth, spindle speed, feed speed, and the ultrasonic field influence grinding force is of significant importance. Such analysis provides vital guidance for identifying optimal processing windows. Figs. 5(a), (b), and (c) illustrate the specific effects of these parameters on grinding forces under both CG and UAG conditions.

Fig. 5(a) illustrates the influence of grinding depth on grinding forces. For both CG and UAG, forces rise positively with depth. Tangential forces in both methods follow a near-linear trend. However, the normal force in CG shows no obvious upward trend below 30 μm. Beyond this critical value, its growth rate increases noticeably. Interestingly, in the 30–40 μm range, the linear behavior of CG aligns with that of UAG. Despite this similarity, UAG maintains a clear advantage, lowering normal and tangential forces by 24.16% and 21.12%, respectively. This reduction stems primarily from the ultrasonic softening effect. As grinding depth increases, the volume of material engaged grows substantially. In CG, this naturally leads to a rapid accumulation of cutting resistance. UAG, however, behaves differently. The high-frequency vibration promotes micro-crack propagation in SiC particles ahead of the tool.

This creates a "pre-damage" zone that effectively lowers the material's yield limit. Consequently, the sharp rise in forces typically seen at greater depths is significantly curbed.

Fig. 5(b) plots grinding forces against feed speed. As speed increases, a positive correlation is observed for both CG and UAG. The evolution of normal and tangential forces remains nearly identical across both methods. Within the experimental parameters, UAG demonstrates a definitive advantage. It suppresses normal and tangential forces by approximately 12.8% and 23.5%, respectively. The reason lies in the interplay between chip thickness and contact dynamics. Higher feed speeds increase the undeformed chip thickness (UCT), which intensifies the load on individual grains. UAG counteracts this through its inherent intermittent separation, which cuts down the effective friction time between tool and workpiece. Moreover, the ultrasonic impact fragments SiC particles more efficiently. This action offsets the cumulative resistance caused by faster feeding, keeping UAG forces consistently lower than those in CG.

Fig. 5(c) illustrates the impact of spindle speed. Unlike the monotonic trend seen with depth, forces here initially decline before ascending. In the 13.09-23.56 $m \cdot s^{-1}$ range, the machining method exerts negligible influence on normal force. Tangential force trends remain consistent, with UAG achieving a reduction of roughly 26%. Above 23.56 $m \cdot s^{-1}$, the normal force in UAG stabilizes. While other components increase at varying rates, UAG retains a substantial lead throughout the entire range. The initial drop in force is driven by a reduction in single-grain chip thickness at higher speeds. However, as speed climbs further, friction and heat can cause forces to rise again. UAG handles this better by improving chip evacuation and reducing thermal buildup. At the microscopic level, superimposing ultrasonic velocity onto the high spindle speed amplifies the instantaneous impact force. This facilitates easier particle removal, helping to stabilize forces even when the spindle runs at high rpms.

Overall, data in Fig. 5 confirms that UAG consistently yields lower forces than CG. This performance gap stems from altered cutting kinematics. UAG reduces both the effective cutting time and the average undeformed chip thickness, thereby lowering resistance. Furthermore, the intermittent "contact-separation" cycle induces an impact effect on SiC particles. This modifies the material removal mechanism. Specifically, it promotes micro-fracture, reducing the specific energy required and, consequently, the grinding forces.

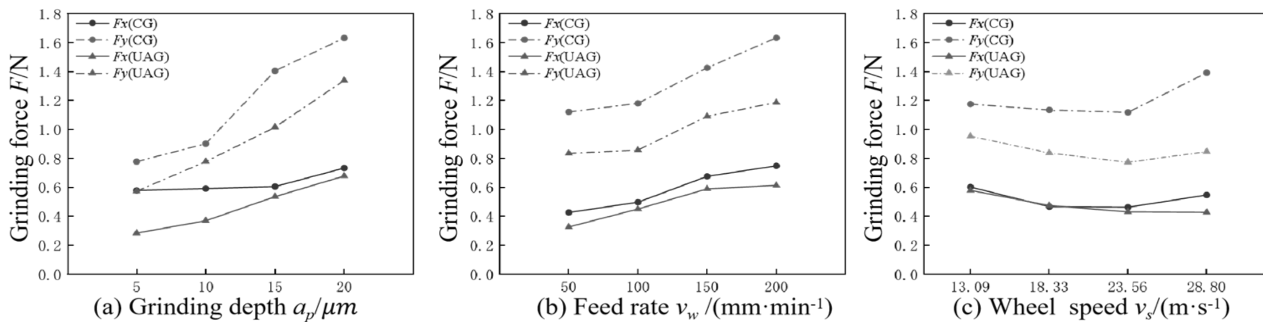

Fig. 5 *Effect of Machining Parameters on Grinding Force photograph*

3.2 Surface Morphology

Surface damage in high volume fraction SiCp/Al composites comprises SiC particle damage, Al matrix damage, and interface damage. Fig. 6 presents SEM[22] and EDS images captured after CG processing. As observed in Fig. 6, the damage includes particle fracture, interface failure, and tearing or smearing of the Al matrix. During the CG process, SiC particles are primarily removed via brittle fracture, while the Al matrix exhibits significant plastic flow. The resulting defects, such as pits, voids, and cracks, severely compromise the surface quality.

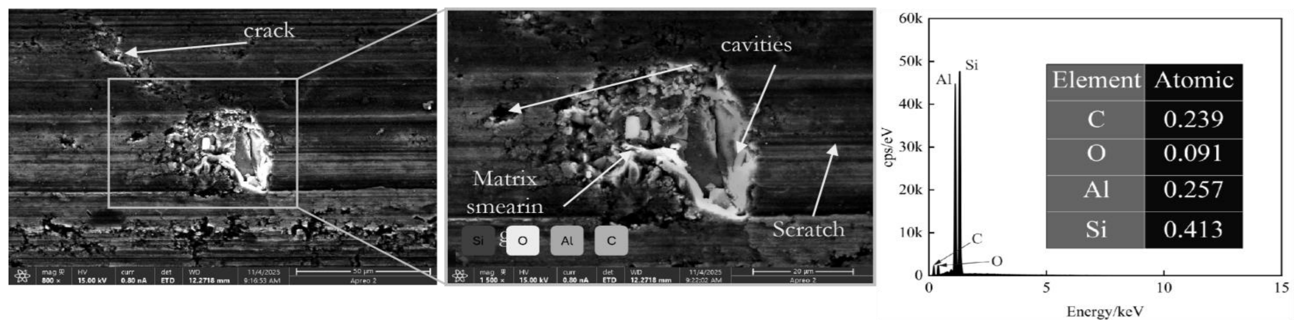

Fig. 6 *SEM and EDS Morphology of Machined Surfaces of High-Volume Fraction SiCp/Al*

Figure 7 presents SEM micrographs of surfaces machined by CG and UAG under identical parameters. In the case of CG, due to the inherent high hardness and brittleness of SiC particles, the cutting force exerted by the abrasive grains often exceeds the particle fracture limit. Consequently, the dominant removal modes are brittle fracture or particle pull-out, resulting in a surface characterized by macroscopic brittle fracture features and pits of varying sizes, as shown in Fig. 7(a). Conversely, under UAG conditions, the intermittent contact characteristics (contact-separation) of ultrasonic vibration reduce the interaction time between the abrasive grains and the particles while also altering the cutting angle. This mechanism effectively decreases the instantaneous single-grain undeformed chip thickness (UCT), transitioning a portion of the SiC removal from the brittle regime to the ductile regime. Furthermore, residual particle fragments tend to fill the voids, thereby enhancing the overall surface quality, as depicted in Fig. 7(b).

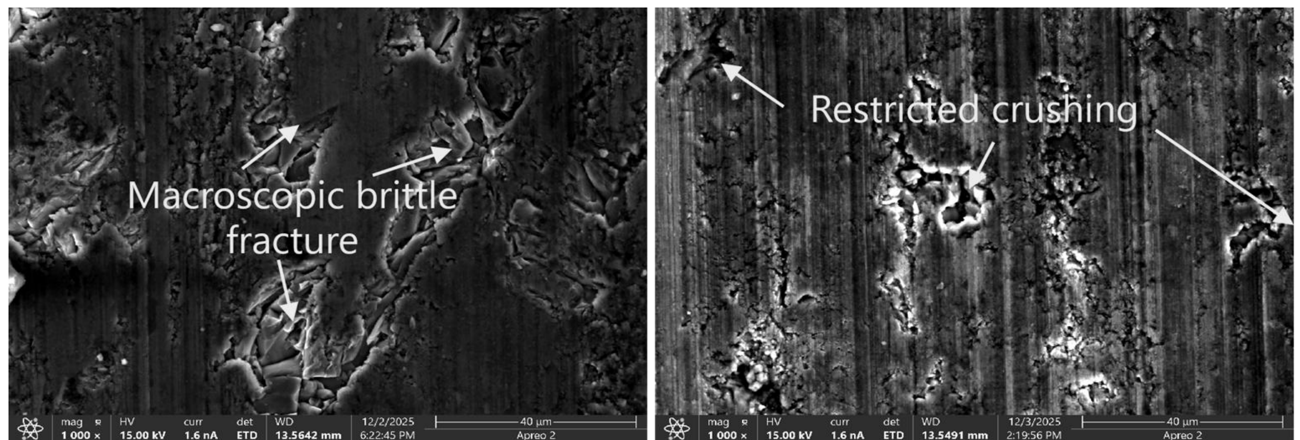

Fig. 7 *Comparison of Machining Damage in CG and UAG under Identical Parameters*

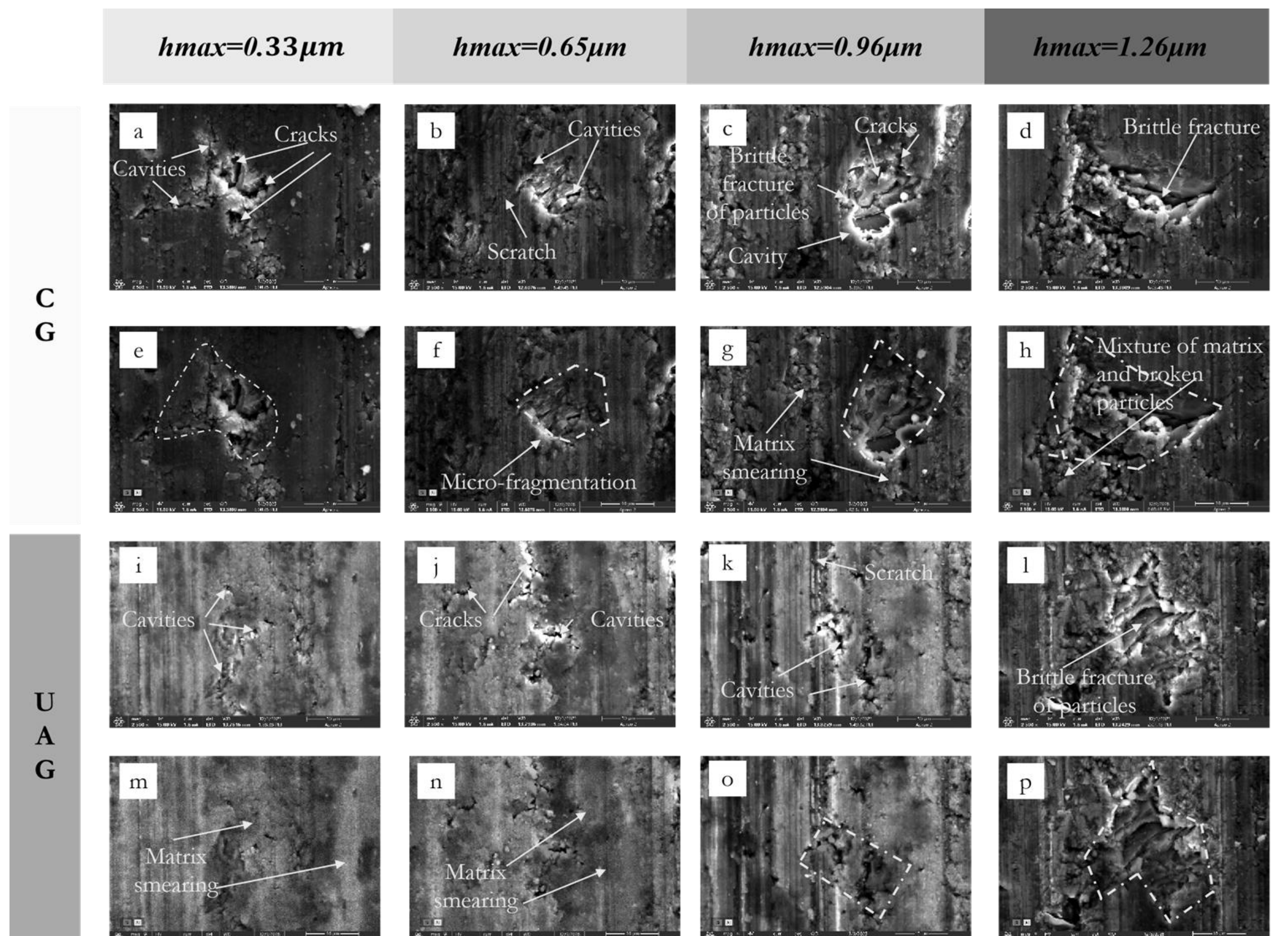

Fig. 8 *SEM and EDS Characterization of Surface Damage Morphology in CG and UAG under Varied UCT Conditions*

Generally, SiC particles tend to undergo ductile removal when the single-grain undeformed chip thickness (UCT) is below a critical threshold, whereas brittle removal dominates once this value is exceeded. Figure. 8 illustrates the surface morphologies of the high volume fraction SiCp/Al composite under both CG and UAG conditions as the UCT increases from 0.3 to 1.2 μm. The specific experimental parameters and corresponding UCT values are detailed in Table 2.

Increasing the maximum undeformed chip thickness (UCT) from 0.3 to 1.2 μm reveals the complete transition of the SiC particle removal mechanism from a ductile-dominated to a brittle-dominated mode. However, a close inspection of Fig. 8 highlights significant discrepancies between conventional grinding (CG) and ultrasonic-assisted grinding (UAG) throughout this evolution. Under identical cutting parameters, the UAG surface maintains superior particle integrity and interface quality, avoiding the premature crushing or detachment observed in the CG process. This indicates that the introduction of ultrasonic vibration shifts the critical threshold for the ductile-to-brittle transition, thereby fundamentally altering the final morphology of surface damage.

Based on the SEM and EDS morphologies obtained at varying UCT values, distinct material behaviors are observed. At a low chip thickness of 0.33 μm, the CG surface (Fig. 8a, e) is characterized primarily by shallow pits but already exhibits signs of slight particle spalling, suggesting an entry into the mixed ductile-brittle removal regime. In contrast, the UAG surface (Fig. 8i, m) retains clear and continuous plastic ploughing striations on the SiC particles with intact edges, demonstrating high-quality ductile removal characteristics. As the UCT increases to the transition range of 0.65–0.96 μm, the morphological divergence between the two processes widens. SiC particles in the CG process begin to undergo macro-fracture and severe interfacial failure, leaving distinct pits on the workpiece surface (Fig. 8f, g). Conversely, UAG exhibits a constrained micro-fracture morphology (Fig. 8n, o); although fractured, the particles remain embedded in the matrix without severe cracking at the interface. Even under the extreme condition of 1.26 μm where brittle fracture dominates, UAG retains a distinct advantage. Unlike the extensive particle fracture and pits found on the CG surface (Fig. 8h), the thermal softening effect induced by ultrasound promotes intense plastic flow of the aluminum matrix, which "smears" over the fractured SiC particles and voids (Fig. 8p). This restorative action effectively fills surface defects, significantly reducing both the depth and area of the pits.

Synthesizing the evolutionary characteristics across these stages, it is evident that UAG offers significantly better protection of particle integrity than CG, regardless of whether the process is in the ductile, mixed, or brittle zone. This phenomenon strongly validates the mechanism illustrated in Fig. 9, ultrasonic-assisted processing effectively expands the critical UCT threshold for the ductile-to-brittle transition of SiC particles. Consequently, within the same UCT range, UAG maintains a higher proportion of ductile or mixed removal modes, thereby shrinking the domain of pure brittle removal. This threshold shift biases particle removal towards micro-crushing rather than macro-fracture or pull-out, effectively limiting the formation of large-scale defects. This explains why UAG yields superior surface quality, even under high-efficiency removal conditions.

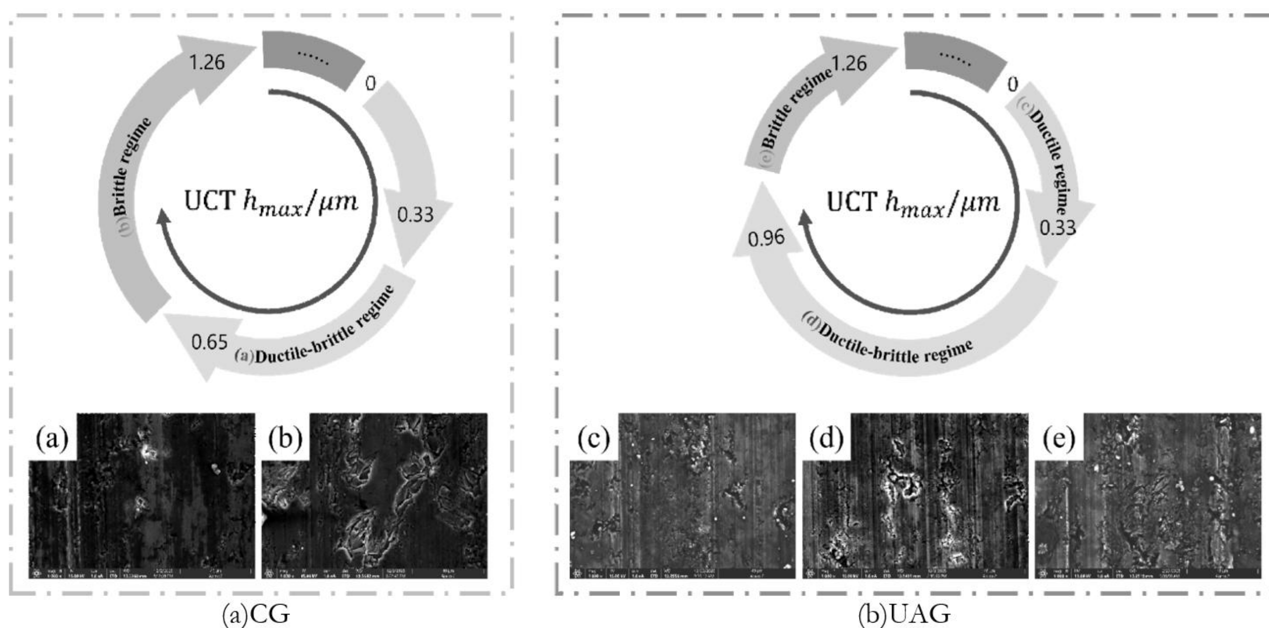

***Fig. 9** Distribution of Material Removal Regimes photograph*

3.3 Surface Roughness

The surface quality of ground composites is largely governed by the removal mode of the SiC particles, with large, deep voids from pure brittle fracture being the main driver of surface degradation. As discussed in Section 3.2, UAG helps suppress such fragmentation by pushing the brittle fracture threshold to higher limits. This leads to a clear improvement in surface integrity; compared to CG under identical parameters, UAG surfaces consistently show fewer and smaller pits. Fig. 10 presents representative 3D topographies selected from the single factor experiments to illustrate this contrast. In these images, the reduction in both the number and size of surface defects is clearly visible, directly explaining the lower roughness values achieved with ultrasonic assistance.

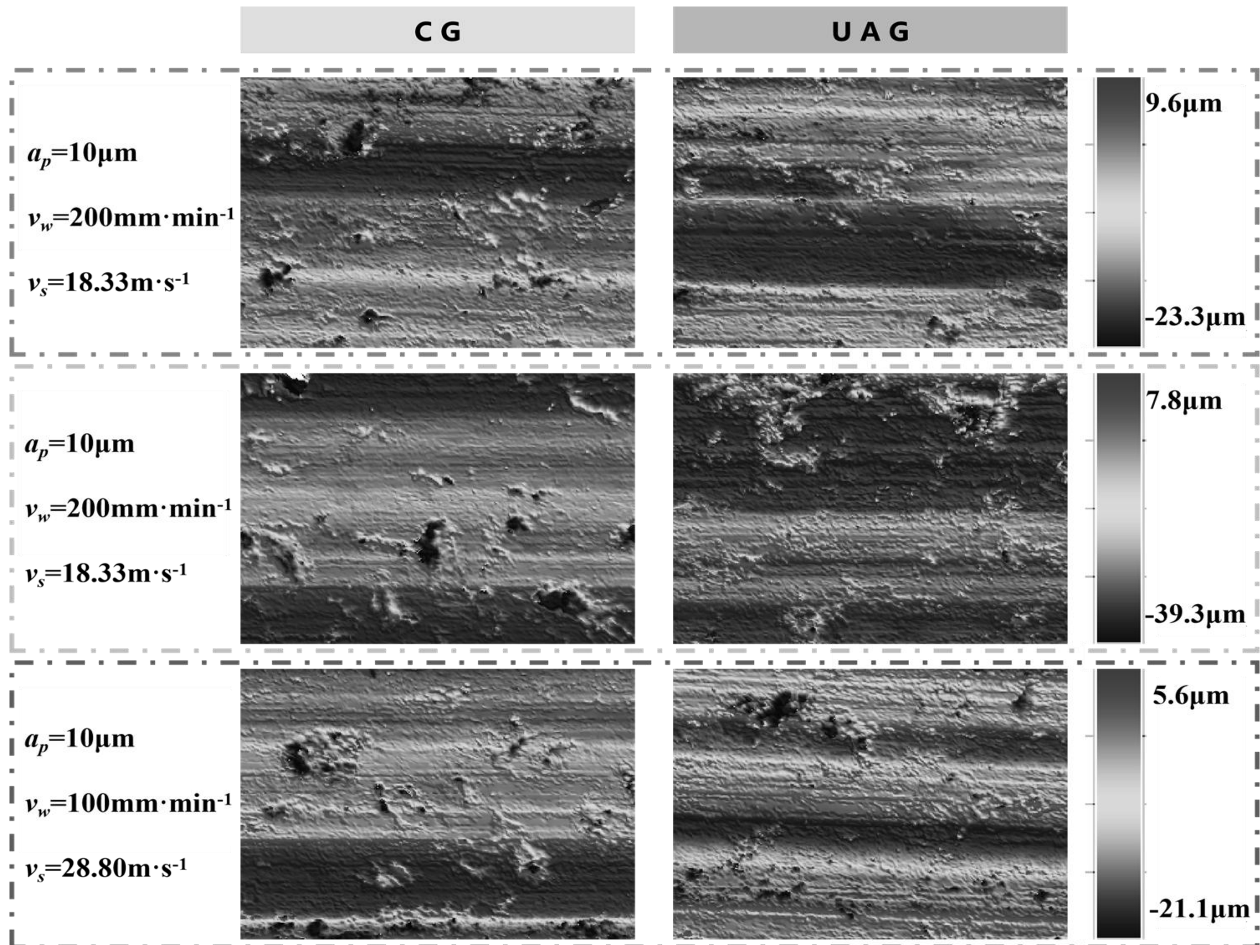

Fig. 10 *3D surface morphology*

The surface roughness results obtained from UAG and CG experiments are illustrated in Fig. 11(a–c) as a function of process parameters. The evolutionary trends for both processes are fundamentally similar, where roughness increases linearly with grinding depth and feed rate, but decreases as the spindle speed increases.

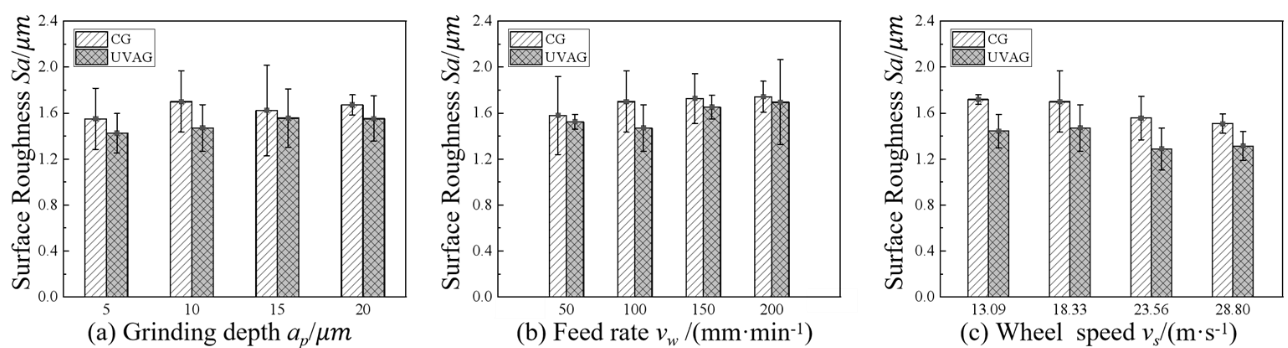

Fig. 11 *Surface Roughness of CG and UAG under Different Grinding Parameters*

Surface roughness increases gradually as grinding depth becomes larger, leading to severe quality degradation, as shown in Fig. 11(a). This trend is driven by the variation in undeformed chip thickness (UCT). At low depths, the UCT is small, placing SiC particles in the ductile or mixed removal regime. Cutting action dominates, resulting in micro-fracture removal with few pits and shallow, uniform matrix grooves. However, as depth increases, the UCT enlarges. This significantly raises grinding forces and induces obvious stress concentration, making particles prone to fracture. Consequently, large-scale debonding and pull-out occur, creating numerous pits, deeper grooves, and cracks. Compared to CG, UAG exhibits a slower roughness growth rate and lower absolute values. This is because UAG reduces the effective UCT and alters the material removal distribution. Even at large depths, particles remain in the mixed removal interval, which suppresses large-scale fragmentation and mitigates morphology deterioration. Thus, UAG demonstrates a significant capability to inhibit particle fracture under large cutting depths.

Surface roughness presents a cumulative, stable rise with increasing feed speed, although the surface morphology shows no significant deterioration (Fig. 11(b)). The underlying cause is the change in single-grain dynamics. As feed speed increases, the cutting zone per unit time lengthens, and the material removal volume per grain grows. With fewer overlapping grinding trajectories, matrix grooves transition from small and shallow to large and deep. Concurrently, increased grinding forces cause stress concentration, leading to gradual particle fracture. For UAG, the increasing trend of roughness is less pronounced than in CG. The application of ultrasonic vibration induces intermittent separation between grain and material, which reduces the grain load per unit time. Additionally, UAG improves the distribution of removal zones. These factors enable UAG to effectively inhibit the cumulative surface damage caused by higher feed speeds.

Surface quality improves stably and roughness values decrease continuously as spindle speed increases, as illustrated in Fig. 11(c). This improvement occurs because higher speeds increase the number of active grains per unit time, creating dense motion trajectories. This weakens the load on individual grains and reduces the effective UCT. Consequently, particle removal modes concentrate in the mixed and ductile intervals, lowering the probability of fracture, debonding, and pull-out, while matrix grooves become shallower. In the case of UAG, the reduction magnitude of roughness is even greater than in CG. The ultrasonic-induced intermittent separation further attenuates the grain load and minimizes the effective UCT. This stabilizes particle removal within the ductile and mixed intervals, thereby optimizing surface morphology. essentially, UAG amplifies the beneficial effect of increasing spindle speed on surface quality.

4 Conclusion

- While grinding forces in both CG and UAG follow similar trends relative to cutting parameters, adding ultrasonic energy causes a clear drop in overall force magnitude. Experimental data show varying degrees of reduction, reaching a maximum decrease of 26% under optimal conditions. Crucially, this reduction is highly sensitive to the ultrasonic settings. In particular, increasing the ultrasonic amplitude proved to be the most significant factor in lowering grinding resistance and enhancing the cutting state.
- Grinding of high volume fraction SiCp/Al composites is prone to defects such as grooves, voids, cracks, particle fracture, and pull-out. Among these, particle damage dominates the surface morphology quality. By reducing the critical undeformed chip thickness (UCT), UAG optimized the distribution of particle removal modes. Consequently, the probability of ductile and mixed removal modes increased, effectively suppressing particle damage.
- A critical threshold exists for grinding depth, beyond which particle damage rapidly transitions into the brittle fracture regime, causing a sharp spike in surface roughness. Feed speed, by contrast, exerts a cumulative deterioration effect on roughness, whereas higher spindle speeds help attenuate single-grain loads, progressively optimizing surface quality. With the superposition of ultrasonic vibration, UAG effectively expands this critical depth threshold and mitigates the damage accumulation driven by higher feed rates. Furthermore, it amplifies the load-reducing benefits of increased spindle speeds. Together, these mechanisms significantly enhance surface integrity, demonstrating that UAG offers superior performance in machining high volume fraction SiCp/Al composites.

Acknowledgement

This article is supported and funded by the National Natural Science Foundation of China (Grant No. 52475478)

References

[1] LIPIŃSKI, T. (2024). Microstructure and mechanical properties AlSi7Mg alloy with Sr, Al and AlSi7Mg. In: *Manufacturing Technology Journal*, Vol. 24, No. 2, pp. 227-234.

[2] LI, Q., YUAN, S., BATAKO, A., CHEN, B., GAO, X., LI, Z., AMIN, M. (2024). Modeling for ultrasonic vibration-assisted helical grinding of SiC particle-reinforced Al-MMCs. In: *The International Journal of Advanced Manufacturing Technology*, Vol. 131, No. 9–10, pp. 5223–5242.

[3] ZHOU, Y., GU, Y., LIN, J., ZHAO, H., LIU, S., XU, Z., YU, H., FU, X. (2022). Finite element analysis and experimental study on the cutting mechanism of SiCp/Al composites by ultrasonic vibration-assisted cutting. In: *Ceramics International*, Vol. 48, No. 23, pp. 35406–35421.

[4] WANG, L., PAN, Y., ZHU, X. (2023). Effect of milling parameters on the surface roughness of SiCp/Al materials. In: *Manufacturing Technology Journal*, Vol. 23, No. 4, pp. 545-550.

[5] ZHOU, J., LU, M., LIN, J., WEI, W. (2023). Influence of tool vibration and cutting speeds on removal mechanism of SiCp/Al composites during ultrasonic elliptical vibration-assisted turning. In: *Journal of Manufacturing Processes*, Vol. 99, pp. 445–455.

[6] WANG, H., ZHANG, H., ZHOU, M., GU, C., BAI, S., LIN, H. (2023). Study of surface defect detection techniques in grinding of SiCp/Al composites. In: *Applied Sciences*, Vol. 13, No. 21, p. 11961.

[7] YAO, X., YU, W., PENG, J., DING, W., ZHAO, B. (2025). Study on ultrasonic vibration-assisted grinding characteristics of high volume fraction SiCp/Al composites. In: *The International Journal of Advanced Manufacturing Technology*, Vol. 138, No. 2, pp. 385–400.

[8] HU, C., ZHU, Y., FAN, R. (2024). Experimental studies of the machinability of SiCp/Al with different volume fractions under ultrasonic-assisted grinding. In: *Materials*, Vol. 17, No. 12, p. 3024.

[9] GU, P., ZHU, C., SUN, Y., WANG, Z., TAO, Z., SHI, Z. (2023). Surface roughness prediction of SiCp/Al composites in ultrasonic vibration-assisted grinding. In: *Journal of Manufacturing Processes*, Vol. 101, pp. 687–700.

[10] JIN, J., MAO, J., WANG, R., CUI, M. (2025). Experimental study on ultrasonic vibration-assisted grinding of SiCp/Al composites grinding. In: *Micromachines*, Vol. 16, No. 3, p. 302.

[11] YUAN, Z., XIANG, D., PENG, P., ZHANG, Z., LI, B., MA, M., ZHANG, Z., GAO, G., ZHAO, B. (2023). A comprehensive review of advances in ultrasonic vibration machining on SiCp/Al composites. In: *Journal of Materials Research and Technology*, Vol. 24, pp. 6665–6698.

[12] ZHOU, Y., TIAN, C., JIA, S., MA, L., YIN, G., GONG, Y. (2023). Study on grinding force of two-dimensional ultrasonic vibration grinding 2.5D-C/SiC composite material. In: *Crystals*, Vol. 13, No. 1, p. 151.

[13] ZHANG, K., DAI, C., YIN, Z., MIAO, Q., CHEN, J., CHENG, Q., YANG, S. (2024). Modeling and prediction on grinding force in ultrasonic assisted elliptical vibration grinding (UAEVG) of SiC ceramics using single diamond grain. In: *Journal of Manufacturing Processes*, Vol. 131, pp. 2244–2254.

[14] GAO, X., AN, W., WANG, L., CHEN, B., XU, W., FENG, Q., LI, Q., YUAN, S. (2024). Study on the critical conditions for ductile-brittle transition in ultrasonic-assisted grinding of SiC particle-reinforced Al-MMCs. In: *Ceramics International*, Vol. 50, No. 24, pp. 52742–52760.

[15] CHENG, Q., DAI, C., MIAO, Q., YIN, Z., CHEN, J., YANG, S. (2024). Undeformed chip thickness with composite ultrasonic vibration-assisted face grinding of silicon carbide: Modeling, computation and analysis. In: *Precision Engineering*, Vol. 86, pp. 48–65.

[16] LI, Y., YANG, Y., XIONG, J., PENG, P., XIANG, D. (2025). Modelling of ultrasonic grinding force considering the wheel topography generated by rotary dressing operation. In: *The International Journal of Advanced Manufacturing Technology*, Vol. 140, No. 3–4, pp. 1485–1503.

[17] YING, J., YIN, Z., ZHANG, P., ZHOU, P., ZHANG, K., LIU, Z. (2022). An experimental study of the surface roughness of SiCp/Al with ultrasonic vibration-assisted grinding. In: *Metals*, Vol. 12, No. 10, p. 1730.

[18] ZHOU, J., LU, M., LIN, J., ZHOU, X., GUO, M., DU, Y. (2022). Investigation of surface integrity transition of SiCp/Al composites

based on specific cutting energy during ultrasonic elliptical vibration assisted cutting. In: *Journal of Manufacturing Processes*, Vol. 79, pp. 654–665.

[19] YAO, X., PENG, J., ZHOU, R., WANG, R., LI, G., DING, W., ZHAO, B. (2025). Material removal and damage formation mechanisms during ultrasonic vibration-assisted grinding of high volume fraction SiCp/Al composites. In: *Precision Engineering*, Vol. 96, pp. 625–639.

[20] CHARDE, M. M., NAJAN, T. P., CEPOVA, L., JADHAV, A. D., RASHINKARD, N. S., SAMAL, S. P. (2025). Predictive modelling of surface roughness in grinding operations using machine learning techniques. In: *Manufacturing Technology Journal*, Vol. 25, No. 1, pp. 14-23.

[21] ZHU, C., GU, P., WU, Y., LIU, D., WANG, X. (2019). Surface roughness prediction model of SiCp/Al composite in grinding. In: *International Journal of Mechanical Sciences*, Vol. 155, pp. 98–109.

[22] KNAST, P., PETRŮ, J., LEGUTKO, S., SOOS, L., POKUSOVA, M. (2025). SEM analysis of surface layers with variable Ra parameters for tribological optimization in design engineering. In: *Manufacturing Technology Journal*, Vol. 25, No. 2, pp. 185-201.